Highly Active, Durable, and Ultra-Low-Platinum-Group-Metal Nanostructured Thin Film Oxygen Reduction Reaction Catalysts and Supports

Andrew Steinbach (Primary Contact), Cemal Duru, Andrew Haug, Monika Kuznia, Krzysztof Lewinski, Jason Petrin, Grant Thoma, David Rowe, Cedric Bedoya, Jim Phipps, Michael Stephens, and Jason Bender
3M Company, Corporate Research Laboratory
3M Center, Building 201-1W-28
St. Paul, MN 55144-1000
Phone: (651) 737-0103
Email: ajsteinbach2@mmm.com

DOE Manager: David Peterson
Phone: (720) 356-1747
Email: David.Peterson@ee.doe.gov

Technical Advisor: John Kopasz
Argonne National Laboratory
Phone: (630) 252-7531
Email: kopasz@anl.gov

Contract Number: DE-EE0007270

Subcontractors:
- Johns Hopkins University, Baltimore, MD
- Purdue University, West LaFayette, IN
- Oak Ridge National Laboratory, Oak Ridge, TN
- Argonne National Laboratory, Lemont, IL

Project Start Date: January 1, 2016
Project End Date: June 30, 2019

Overall Objectives

The overall objective is development of improved thin film oxygen reduction reaction (ORR) catalysts on nanostructured thin film (NSTF) supports that achieve:

- Mass activity of 0.50 A/mg_{PGM} or more
- Platinum-group metal (PGM) total content (both electrodes) of ≤0.1 g/kW
- PGM total loading (both electrodes) <0.1 mg_{PGM}/cm^2
- Mass activity durability of <20% loss
- Loss of performance <20 mV @ 0.8 and 1.5 A/cm^2.

Fiscal Year (FY) 2018 Objectives

- Develop new ultra-thin film (UTF) toward achievement of activity, durability, and cost objectives.
- Employ advanced composition and structural analysis to guide electrocatalyst development, including transmission electron microscopy, energy dispersive X-ray spectroscopy (EDS), and X-ray adsorption fine structure spectroscopy (XAFS).
- Utilize density functional theory (DFT) and kinetic Monte Carlo (KMC) models to predict novel electrocatalyst concepts with improved activity and durability.

Technical Barriers

This project addresses the following technical barriers from the Fuel Cells section of the Fuel Cell Technologies Office Multi-Year Research, Development, and Demonstration Plan[1]:

(A) Durability

(B) Cost

(C) Performance.

Technical Targets

Table 1 summarizes 2018 project status against the relevant 2020 DOE targets and project targets. All reported status values are measurements made in membrane electrode assembly (MEA) format.

This year, two individual project electrocatalysts were demonstrated. They exceed five of the six 2020 targets that this project addresses and have met three of six of the more stringent project targets. The electrocatalysts are based on a

[1] https://energy.gov/eere/fuelcells/downloads/fuel-cell-technologies-office-multi-year-research-development-and-22

stabilized, layered catalyst structure consisting of a surface Pt layer and an "underlayer" of Ir between the Pt surface layer and the NSTF perylene red 149 whisker support. The first catalyst, which comprised 50 $\mu g_{Pt}/cm^2$ and 11 $\mu g_{Ir}/cm^2$, demonstrated a PGM total content of 0.110 g_{PGM}/kW, a PGM total loading of 0.098 mg/cm^2, loss in catalytic (mass) activity of 20%, loss in performance at 0.8 A/cm^2 of 22 mV, and loss in performance at 1.5 A/cm^2 of less than 5 mV. The mass activity of this catalyst was 0.29 A/mg_{PGM}, below the DOE target of 0.44 A/mg. The second catalyst, which comprised 31 $\mu g_{Pt}/cm^2$ and 26 $\mu g_{Ir}/cm^2$, demonstrated a PGM total content of 0.106 g_{PGM}/kW, a PGM total loading of 0.094 mg/cm^2, loss in catalytic (mass) activity of 16%, loss in performance at 0.8 A/cm^2 of 25 mV, and loss in performance at 1.5 A/cm^2 of less than 5 mV. The mass activity of this catalyst was 0.27 A/mg_{PGM}, below the DOE target of 0.44 A/mg_{PGM}.

Project status values for mass activity are provided by three catalysts. Two layered catalysts—one with an Ir underlayer and the second with a Ta underlayer—yielded PGM mass activities of 0.41 A/mg_{PGM} and 0.42 A/mg_{PGM}, respectively, approaching the DOE target. A third catalyst, consisting of a UTF PtNi alloy with a chromium surface additive, achieved 0.57 A/mg_{PGM}—exceeding DOE and project targets.

FY 2018 Accomplishments

- Identified four surface additives—Ir, Ta, Ru, and Cr—that enhance the mass and specific activities of UTF PtNi catalysts within narrow composition ranges. Each of these catalysts met or exceeded the DOE activity target.
- Developed new class of UTF layered Pt/Ir catalysts that resulted in the achievement of five of six DOE targets and three of six project targets. Of note, several Pt/Ir catalysts were demonstrated to have durability that exceeded the DOE 2020 targets by 50% or more, and two Pt/Ir layered catalysts yielded specific power densities that exceeded the DOE target by about 15% to 20%, with ultra-low-PGM areal loadings below the DOE target.
- Developed a new class of UTF layered catalysts that replace Ir with lower-cost, non-precious metals, including Ta. Layered Pt/Ta catalysts with improved process parameters have resulted in up to a 4-fold gain in mass activity relative to the baseline process parameters, achieving 0.42A/mg_{PGM}.
- Tracked subnanometer morphological and compositional changes in literally dozens of Pt-based UTF catalysts using high-throughput, combinatorial electron microscopy methods.
- DFT simulations were utilized to clarify the mechanism of the enhanced stability and activity of Pt/Ir in comparison with Pt. Additionally, DFT simulations provided insights for the choice of underlayer materials with improved adhesion and wetting to enable increased specific area and durability of the catalysts.
- A KMC model of Pt oxidation, reduction, and surface diffusion has been developed, providing insight into several of the surface processes occurring during an accelerated durability cycle.

Table 1. Status Compared with Technical Targets

Characteristic	2020 Target and Units	Project Target	2018 Status
PGM total content (both electrodes)	0.125 g/kW ($Q/\Delta T \leq 1.45$)	0.10	0.110[a] 0.106[b]
PGM total loading (both electrodes)	0.125 mg/cm^2	0.10	0.098[a] 0.094[b]
Loss in catalytic (mass) activity	40%	20	20[c] 16[d]
Loss in performance at 0.8 A/cm^2	30 mV	20	22[c] 25[d]
Loss in performance at 1.5 A/cm^2	30 mV	20	<5[c,d]
Mass activity @ 900 $mV_{iR\text{-}free}$	0.44 A/mg	0.50 (in MEA)	0.41[e] 0.42[f] 0.57[g]

[a] 2018 UTF best of class (BOC) MEA with UTF 50Pt/11Ir/NSTF cathode.

[b] 2018 UTF BOC MEA with UTF 31Pt/26Ir/NSTF cathode. BOC MEAs include low-PGM anode (UTF 9Pt/11Ir/NSTF), 14-µm-thick supported perfluorosulfonic acid membrane, and robustness-optimized diffusion media with a cathode interlayer (16 $\mu g_{Pt}/cm^2$).

[c] UTF 50Pt/11Ir.

[d] UTF 31Pt/26Ir.

[e] UTF 28Pt/12Ir; UTF 10Pt/Ta.

[f] UTF 28PtNi+Cr.

[g] PGM content values at 95°C cell, 150 kPa hydrogen/air, 2.0 and 2.5 hydrogen and air stoichiometry, and $Q/\Delta T$ = 1.45 kW/°C (0.663 V).

INTRODUCTION

State-of-the-art proton exchange membrane fuel cell (PEMFC) membrane electrode assemblies utilized in today's prototype automotive traction fuel cell systems continue to suffer from key technical and economical limitations, including high cost, insufficient durability, and low robustness to off-nominal operating conditions. Many state-of-the art MEAs based on conventional carbon-supported Pt nanoparticle catalysts currently incorporate precious metal loadings that are significantly greater than those needed to achieve MEA cost targets; however, performance, durability, and robustness decrease significantly as loadings are reduced.

This project focuses on development of novel thin-film electrocatalysts based on 3M's NSTF catalyst technology platform. NSTF electrocatalysts and electrodes provide a unique approach toward addressing key technical challenges toward commercialization. The thin film–electrocatalyst structure imparts substantially high ORR specific activities and high resistance to electrocatalyst dissolution and sintering induced by electrochemical cycling [2]. The NSTF support is based on an oriented, submicron-scale crystalline organic pigment whisker—not carbon nanoparticles—which enables exceptional resistance to corrosion in fuel cell and water electrolysis applications [3]. NSTF electrodes are a single layer of NSTF electrocatalyst particles partially embedded into an ion-conducting membrane. They are ultrathin (<1 μm) and do not require ionomer for proton conduction [4]. When integrated into state-of-the-art operationally robust MEAs, the NSTF electrode structure enables high absolute and specific power densities [1].

APPROACH

The project approach is to establish relationships between electrocatalyst functional response (activity, durability), physical properties (bulk and surface structure and composition), and fabrication processes (deposition, annealing, dealloying) via systematic investigation. Additionally, the project utilizes electrocatalyst modeling and advanced physical characterization to guide and accelerate development.

RESULTS

Previously, we reported results from several series of experiments with the objective of assessing the impacts of composition and structure—induced by processing—on the resultant activity and durability for a range of binary alloy electrocatalysts on NSTF supports. These catalysts comprised one of two morphologies, nanoporous thin film or ultrathin film [5]. Additionally, we reported that addition of Ir to the surface of Pt and PtNi catalysts resulted in both increased mass activity and improved electrocatalyst durability, especially stabilization of specific surface area. Such work resulted in demonstration of several catalysts, which met or substantially approached the DOE mass activity and activity durability targets. This year, electrocatalyst development has focused on furthering the activity, durability, and MEA performance of ultrathin film catalysts.

In one area of work, several additional surface additive candidates were assessed for impact on the activity and durability of UTF PtNi. For each surface additive candidate, a short rollgood of UTF PtNi catalyst with areal Pt loadings of approximately 28–30 $\mu g/cm^2$ was fabricated and sectioned. A different amount of additive was deposited onto the surface of each section. All catalysts were integrated into MEAs and tested at least in duplicate. Figure 1 (left and middle) summarizes the dependence of PGM mass activity of UTF PtNi with surface additive levels of Ir, Au, Ta, and Ru and surface additives Cr, β, δ, and π, respectively. Near 1 at% additive, Ir, Au, Ta, and Ru yielded increased mass activities relative to the 0 additive controls. In contrast, Cr surface additive did not enhance activity near 1 at%, but a large and sharp peak in mass activity—reaching 0.57 A/mg_{PGM}—was obtained near 6 at%. Surface additives β, δ, and π generally decreased mass activity monotonically as additive level was increased from 0.5 up to approximately 10 at%.

Figure 1 (right) summarizes the influence of either Ir or Ta surface additive level on H_2/air performance loss after the DOE electrocatalyst accelerated stress test (AST) at 0.32 A/cm^2. Both surface additives were effective at increasing H_2/air performance durability, but less Ta additive was required than Ir to achieve similar durability.

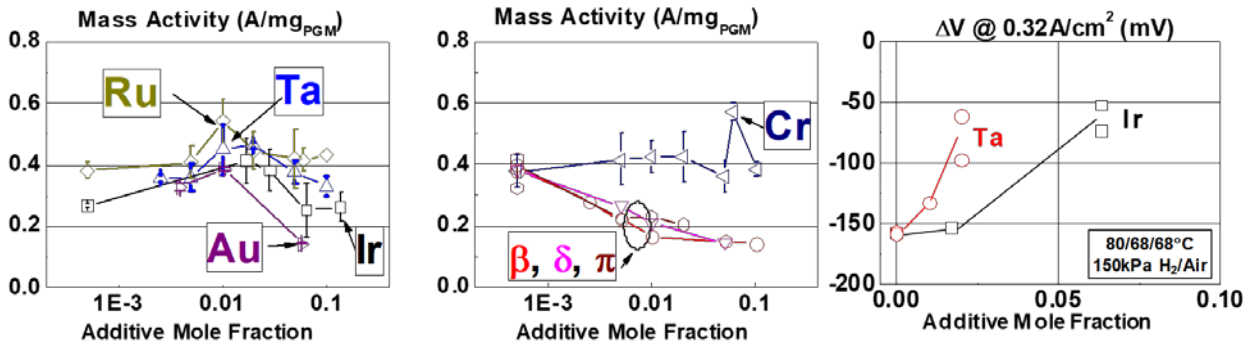

Figure 1. (Left, Middle): Influence of surface additive type and content on PGM mass activity. (Right): Dependence of Ir or Ta surface additive content on H_2/air performance change after the electrocatalyst AST.

In a second major focus area, UTF catalysts were integrated with "underlayers"—layers between the surface ORR catalyst and NSTF perylene red 149 whisker support. Key objectives of the underlayer development included improving the adhesion and wetting of the surface ORR catalyst (relative to direct adhesion to PR149) to enable increased specific area and durability at nanometer-scale catalyst thickness, and to enable increased "support" surface area to allow generation of ultrathin ORR catalyst coatings at reasonable areal electrode loadings near 50 $\mu g_{PGM}/cm^2$. Underlayer development has included assessment and optimization of precious metals, including Ir, and non-precious metal layers comprising Ta.

Figure 2 summarizes the results of several experiments assessing the impact of Ir underlayers with a range of areal loadings (equivalent to thickness on NSTF support) with fixed surface Pt catalyst layer loadings of 5 $\mu g_{Pt}/cm^2$, 10 $\mu g_{Pt}/cm^2$, 28 $\mu g_{Pt}/cm^2$, and 47 $\mu g_{Pt}/cm^2$. For reference, data for pure Pt UTF catalysts at a comparable range of Pt loadings also is shown. Integration of Ir underlayers generally resulted in significantly increased PGM mass activity and specific surface area versus pure Pt, and in some cases enhanced specific activity also was observed (top row). PGM mass activity as high as 0.41 A/mg_{PGM} was obtained at to-date optimal Pt and Ir contents of 28 $\mu g/cm^2$ and 12 $\mu g/cm^2$, respectively. The Ir underlayers also generally increased H_2/air performance, as summarized in Figure 2 (bottom). Depending upon the specific composition, Pt/Ir layered catalysts resulted in increased performance by 10s of millivolts relative to pure Pt at similar PGM areal loadings. At 20 mA/cm^2, 28 Pt/12 Ir (40 $\mu g_{PGM}/cm^2$) yielded a 30 mV gain over Pt with 98 $\mu g_{PGM}/cm^2$.

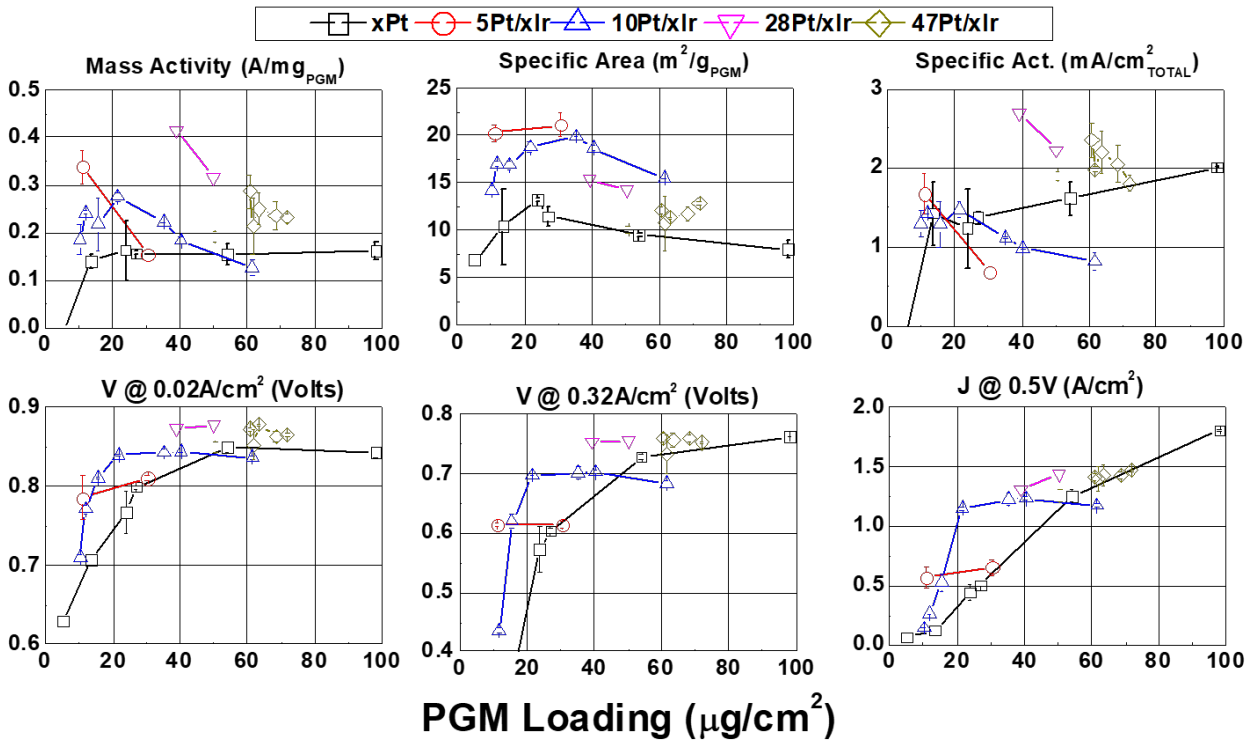

Figure 2. Layered Pt/Ir/NSTF summary. (Top): Mass activity, specific area, and specific activity. (Bottom): H_2/air performances at 0.02 A/cm², 0.32 A/cm², and 0.5 V.

In another series, Pt/Ir/NSTF layered catalysts were prepared with fixed Ir underlayer content and varying surface Pt layer loadings. The top row of Figure 3 summarizes the Pt mass activity and specific activity of xPt/26Ir/NSTF catalysts, revealing extremely high Pt utilization at low Pt contents. This is evidenced by Pt mass activity exceeding 1 A/mg$_{Pt}$ with Pt areal loadings of between 1.1 μg/cm^2 and 4.2 μg/cm^2. A subset of Pt/Ir/NSTF layered catalysts were evaluated by X-ray absorption spectroscopy (Figure 3, bottom). Pt-Pt bond lengths of 9Pt/26Ir/NSTF and 19Pt/26Ir/NSTF were relatively stable throughout fabrication and fuel cell testing and were slightly compressed relative to bulk Pt (2.77Å, not shown). Ir-Ir bond lengths did not depend on surface Pt loading and were similar to bulk Ir.

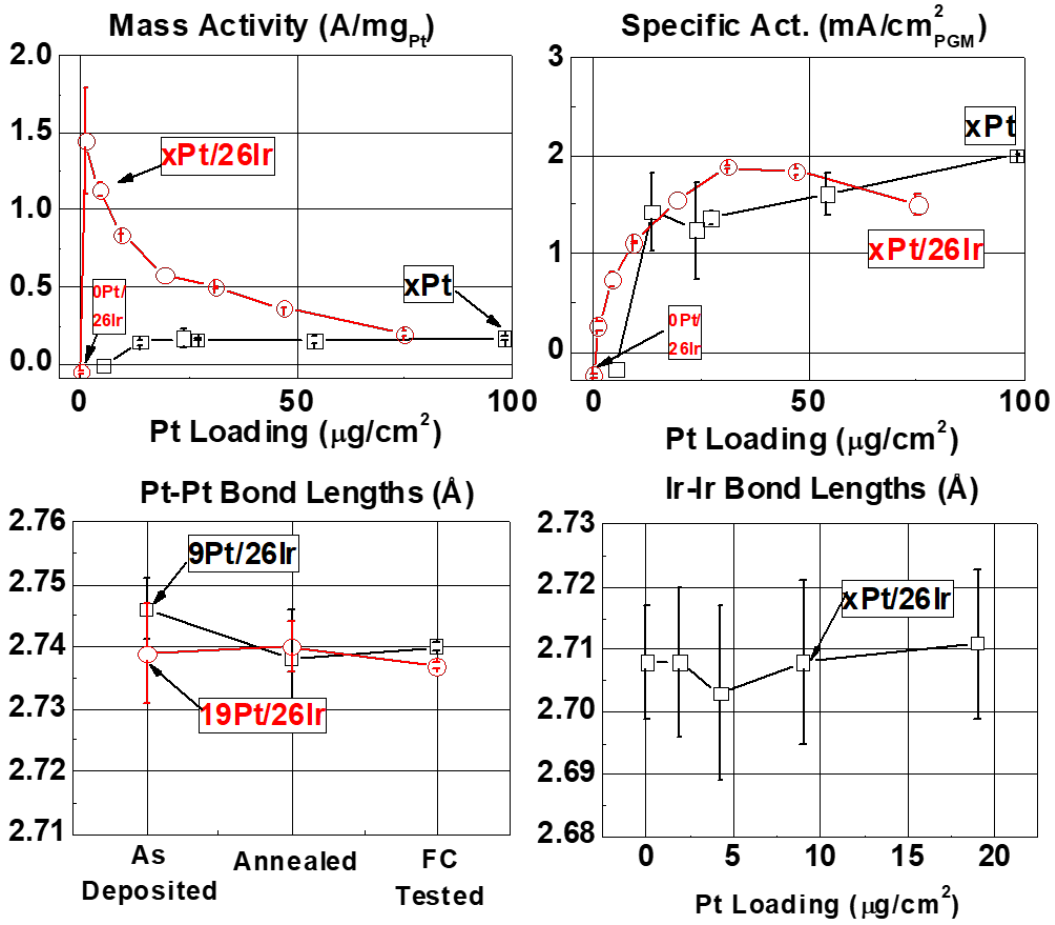

Figure 3. Characterization of Pt and Pt/Ir catalysts with varying surface Pt content. (Top): Mass and specific activities. (Bottom): XAFS-determined bond lengths.

Pt/Ir layered catalysts were assessed for electrocatalyst AST durability. Figure 4 compares H_2/air performance before and after the electrocatalyst AST for three different Pt/Ir/NSTF catalysts with a range of PGM loadings between 35 $\mu g_{PGM}/cm^2$ and 61 $\mu g_{PGM}/cm^2$ (top row) to the performances of Pt alloy nanoparticles on carbon support with 90 $\mu g_{PGM}/cm^2$ electrode loading (bottom left), Pt/NSTF with 54 $\mu g_{PGM}/cm^2$ (bottom center), and PtCoMn/NSTF with 150 $\mu g_{PGM}/cm^2$ (bottom right). The insets in each panel also list the average mass activity and specific area losses. In general, the Pt/Ir/NSTF layered catalysts were significantly more durable than the Pt-alloy nanoparticle catalysts and Pt/NSTF, as evidenced by relatively small downward shifts in the polarization curves (reflective of mass activity losses ranging from 4% to 21% versus the 40% DOE target) and essentially no change in the current density at low cell voltages (reflective of the low specific-area losses, ranging from 3% to 6%). In comparison, the Pt alloy nanoparticle catalyst's mass activity and specific area losses were 66% and 74%, respectively, and the Pt/NSTF losses were 52% and 27%. The performance durability of the Pt/Ir catalyst was qualitatively similar to the relatively high loaded PtCoMn/NSTF catalyst.

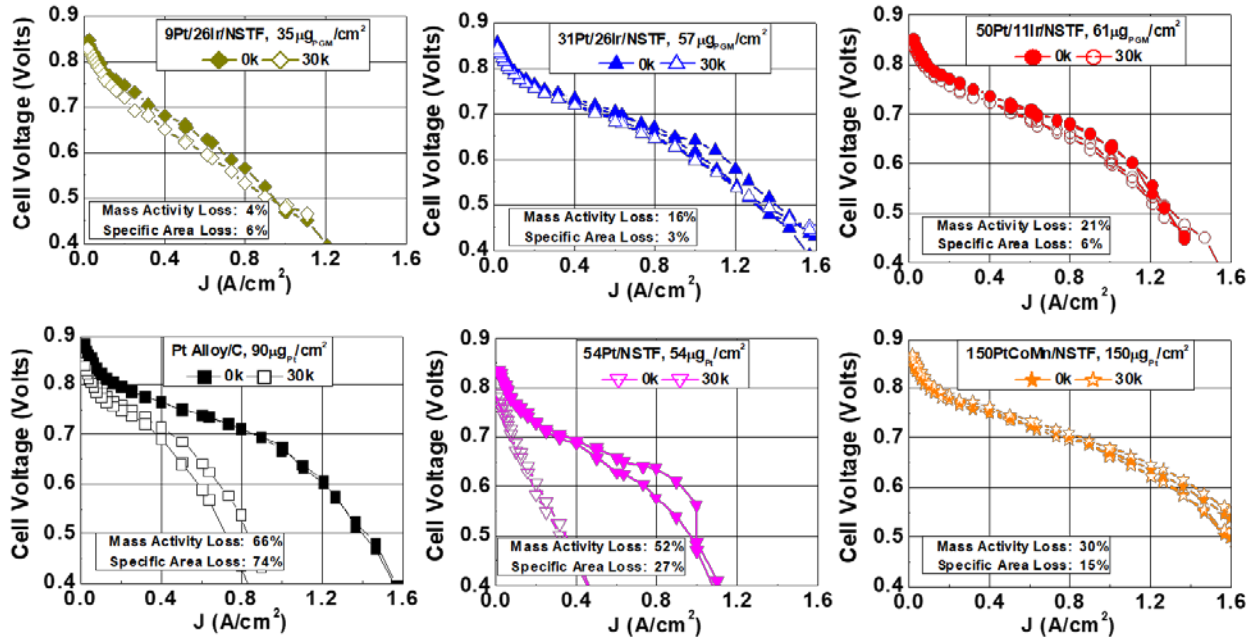

Figure 4. H_2/air polarization curves taken before and after the electrocatalyst AST with Pt/Ir/NSTF catalysts (top), Pt-alloy nanoparticle catalyst on carbon (bottom left), Pt/NSTF catalyst without an Ir underlayer (bottom center), and high loaded PtCoMn/NSTF (bottom right).

In addition to providing stable electrochemical performance, limited studies indicate that the Pt/Ir/NSTF catalysts are compositionally and structurally stable. Figure 5 summarizes complementary high-angle annular dark-field scanning transmission electron microscopy and electron dispersive X-ray spectrum (EDS) images of 10Pt/12Ir/NSTF catalysts before and after the electrocatalyst AST. Prior to the AST, the catalyst consists of a conformal and continuous ~2 nm-thick coating of Pt on a ~2 nm layer of Ir. After testing the catalyst layers remained conformal and continuous on the PR149 whisker support, although some Ir did migrate into and through the surface Pt layer. The EDS-determined Pt and Ir mole fractions remained unchanged within measurement uncertainty.

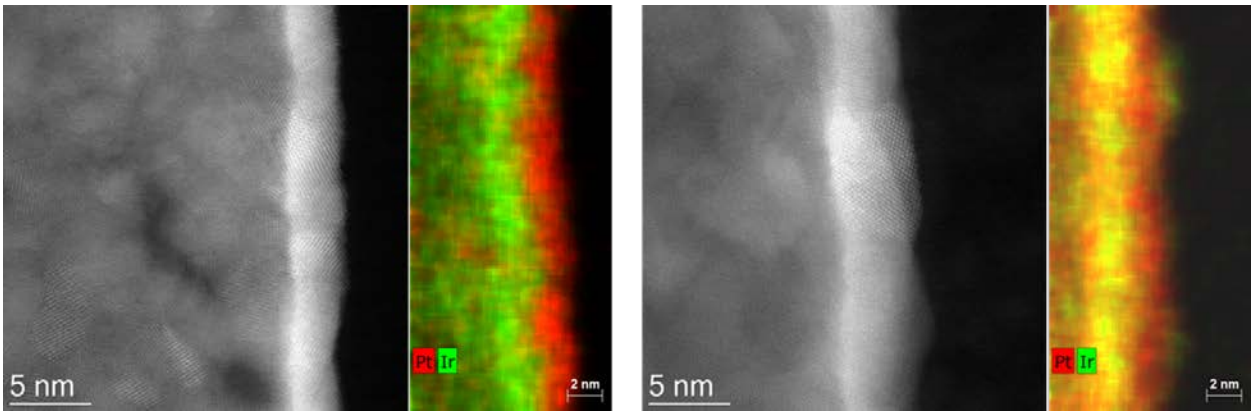

Figure 5. High-angle annular dark-field STEM-EDS of 10Pt/12Ir before electrocatalyst AST (left) and after electrocatalyst AST (right)

Pt/Ir/NSTF catalysts also were assessed for support durability using the DOE Support AST protocol, consisting of 5,000 cycles between 1 V and 1.5 V versus reversible hydrogen electrode, and at 80°C cell temperature. Figure 6 (left) summarizes H_2/air polarization curves taken with 31Pt/26Ir/NSTF before the AST, after 5,000 cycles (target), and after 10,000 cycles. After 5,000 cycles, performance was found to increase by

approximately 100 mV at 1.2 A/cm^2, and an additional 5,000 cycles resulted in a modest further performance increase at higher current densities. Figure 6 (right) shows that the cyclic voltammogram of the cycled cathode essentially is identical to the uncycled cathode, consistent with the estimated <5% loss of specific area. Similar results were obtained with 50Pt/11Ir/NSTF catalyst.

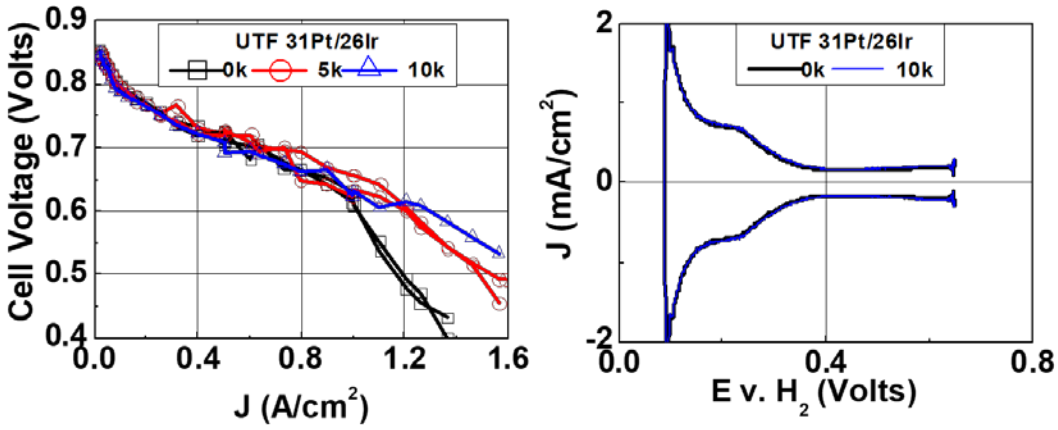

Figure 6. Support AST durability assessment of UTF 31Pt/26Ir; H_2/air polarization curves before and after 5,000 or 10,000 cycles (left); cyclic voltammograms before and after 10,000 cycles (right)

DFT was used to calculate the stability and activity trends of the Pt/Ir catalysts. Figure 7 (left) summarizes the calculated differential formation energy for a range of sub-monolayer Pt coverages on Ir(332) surfaces. Pt sub-monolayers are predicted to be thermodynamically stable on Ir(332) surfaces, as indicated by the negative differential formation energies. Additionally, KMC simulations suggest that Ir could help stabilize Pt via a mechanism in which the less-mobile Ir "pins" Pt in place, slowing structural degradation. Ir therefore is believed to stabilize Pt through a combination of thermodynamic and kinetic effects. In terms of activity, Figure 7 (right) summarizes the predicted oxygen reduction overpotentials and hydroxide binding energies for Pt(111) and a range of Pt overlayers on Ir(111). At Pt layer thicknesses between 3 and 8 monolayers, psueodomorphic Pt on Ir(111) is predicted to have enhanced activity on the order of 20x relative to Pt(111).

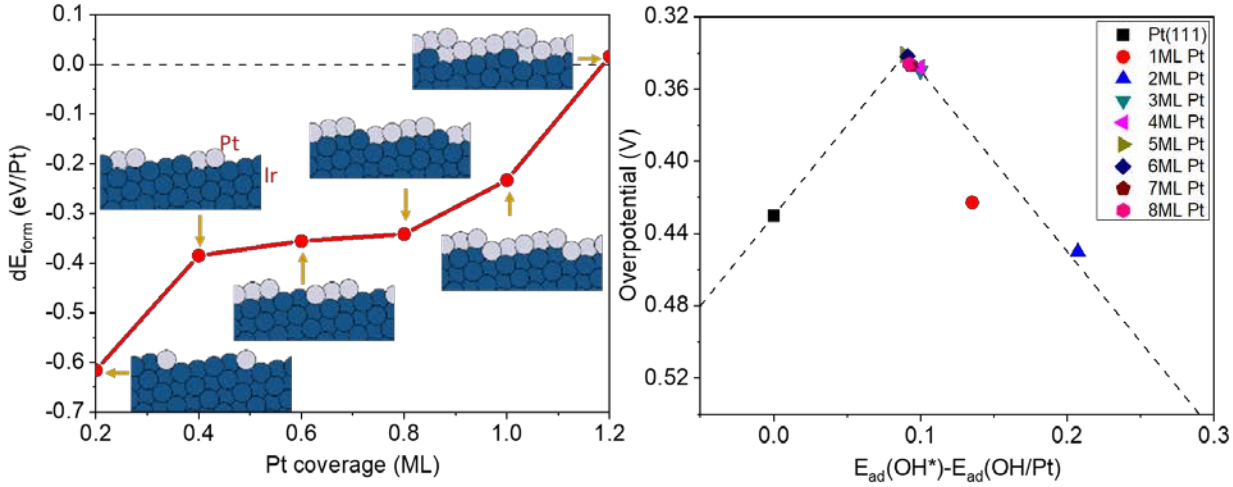

Figure 7. DFT simulations of Pt/Ir. (Left): Differential formation energy for different sub-monolayer coverages of Pt on Ir(332). (Right): Predicted activity of stabilized Pt on Ir(111) as a function of number of Pt monolayers.

Two durable Pt/Ir/NSTF layered catalysts (50Pt/11Ir/NSTF and 31Pt/26Ir/NSTF) were assessed for PGM content and operational robustness in MEAs with "best of class" (BOC) components. Pt/Ir/NSTF layered cathode catalysts were integrated with a high-performance supported 3M 725EW PFSA membrane, a 20

$\mu g_{PGM}/cm^2$ Pt/Ir/NSTF anode catalyst, and a water-permeable anode gas diffusion layer and a cathode gas diffusion layer with a low loaded (16 $\mu g_{PGM}/cm^2$) Pt/C interlayer that improved operational robustness of NSTF MEAs [1]. Total MEA PGM loadings were 0.098 mg/cm^2 and 0.094 mg/cm^2 with the 50Pt/11Ir/NSTF and 31Pt/26Ir/NSTF cathode catalysts, respectively. Figure 8 (left) summarizes the resultant H_2/air performance for replicate MEAs of each type at 95°C cell temperature, 40% relative humidity, and 150 kPa (absolute) pressure. Figure 8 (middle) summarizes performance with 250 kPa (absolute) pressure. At 150 kPa, both Pt/Ir/NSTF layered catalysts achieved similar PGM contents between 0.106 g_{PGM}/kW and 0.110 g_{PGM}/kW at an MEA heat rejection of $Q/\Delta T$=1.45 kW/°C, exceeding the DOE target of ≤0.125 g/kW. At 250 kPa, both Pt/Ir/NSTF catalysts enabled MEA PGM contents of 0.086 g_{PGM}/kW to 0.087 g_{PGM}/kW.

Figure 8 (right) compares steady-state operational robustness of the 2018 NSTF MEAs with total cathode PGM loadings of 73 $\mu g_{PGM}/cm^2$ to 77 $\mu g_{PGM}/cm^2$ to a reference dispersed Pt-alloy nanoparticle on carbon dispersed electrode with 250 $\mu g_{PGM}/cm^2$ cathode loading and to a baseline NSTF MEA (150 $\mu g_{PGM}/cm^2$ cathode) that did not contain the robustness-enhancing anode gas diffusion layer and cathode interlayer. The 2018 BOC MEAs with the Pt/Ir/NSTF cathodes yielded dramatically improved robustness compared to the baseline NSTF MEAs. Under steady-state operation, the 2018 BOC MEAs yield current densities of ca. 0.85A/cm^2 at 33°C, increasing to ca. 1.5 A/cm^2 at about 50°C, vs. the 0.20 to 0.55 A/cm^2 achieved by the baseline NSTF MEA over a similar temperature range. The 2018 BOC MEAs yielded modestly lower performance than the reference Pt-alloy nanoparticle electrode at cell temperature of less than about 45°C.

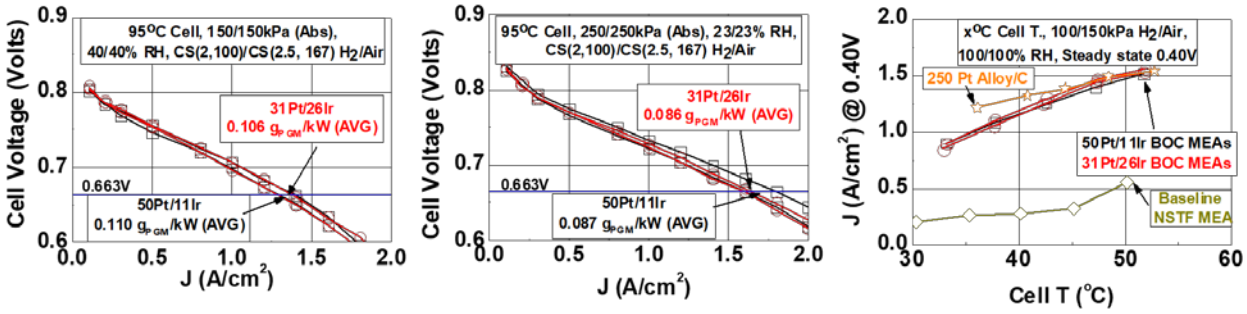

Figure 8. Performance and robustness of 2018 BOC MEAs with either 50Pt/11Ir/NSTF or 31Pt/26Ir/NSTF cathodes. (Left): H_2/air performance at 95°C, 150 kPa. (Center): H_2/air performance at 95°C, 250kPa. (Right): Operational robustness comparisons to baseline NSTF MEA and reference Pt-alloy/C MEA.

In addition to development of catalysts with Ir underlayers, significant research has been conducted toward development of underlayers that have reduced or no precious-metal content. DFT simulations were conducted to assess the adhesion of a variety of underlayers to the PR149 whisker support. Figure 9 summarizes the predicted adhesion of Pt and Ta to a perylene red 149 molecule. Pt is predicted to adhere relatively weakly to PR149, consistent with experimental observations of dewetting. In contrast, Ta is predicted to adhere strongly to PR149, although the impact of Ta oxidation on the adhesion energy remains to be determined. Figure 10 summarizes one set of experiments, where the impact of surface Pt loading was assessed with a fixed Ta underlayer. Pt/NSTF and Pt/Ir/NSTF data is included for reference. As Pt loading on the Ta or Ir underlayers decreased from approximately 80 $\mu g/cm^2$, the PGM mass activity increased, reaching a maximum activity at an intermediate Pt loading of 30 $\mu g/cm^2$ to 40 $\mu g/cm^2$, then decreased toward 0 as the Pt loading decreased below 20 $\mu g/cm^2$. Although the PGM mass activity trends were similar with either underlayer, different trends in specific area and specific activity were observed. With the Ir underlayer, the PGM mass activity decrease below 30 $\mu g/cm^2$ predominantly was because of the loss of specific activity, likely due to a significant contribution of ORR-inactive Ir to the measured surface area and resultant reduction in relative Pt surface area. Additionally, the total measured PGM–specific area increased as the Pt content on Ir was reduced toward zero, likely reflecting the specific area of Ir/NSTF. In contrast, with Ta, the specific area decreased toward 0 as the Pt loading decreased, similar to that observed with Pt directly on the NSTF support.

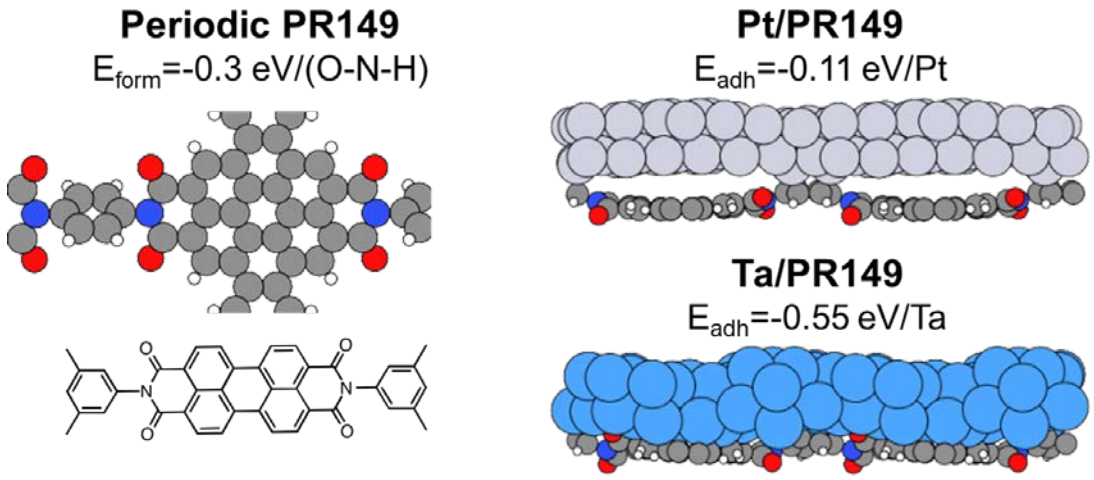

Figure 9. DFT simulations of Pt and Ta adhesion to Perylene Red 149

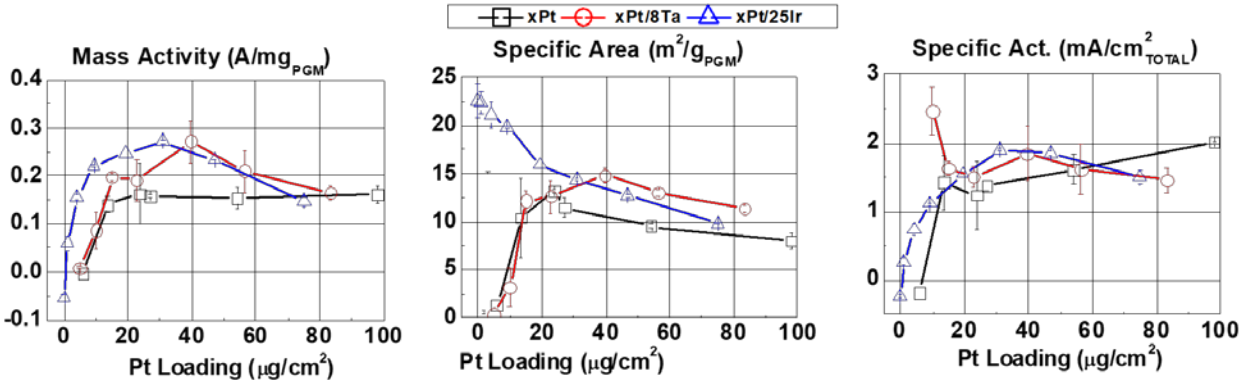

Figure 10. Comparison of PGM mass activity, specific area, and specific activity for xPt/NSTF, xPt/8Ta/NSTF, and xPt/26Ir/NSTF as a function of surface Pt loading

A subset of Pt/Ta/NSTF catalysts was analyzed for composition and structure by STEM, EDS, and XAFS. Figure 11 (left) and (center) compare STEM micrographs for 10Pt/8Ta/NSTF and 20Pt/8Ta/NSTF after fuel cell testing. The 10Pt/8Ta/NSTF consists of discontinuous Pt fibrils on the Ta underlayer, whereas with 20Pt/8Ta/NSTF the Pt layer appeared to be continuous. EDS analysis indicated that the Ta was oxidized, with O:Ta ratios of approximately 1:1. XAFS indicated that the Pt-Pt bond lengths changed only modestly as the surface Pt content on Ta increased from 10 μg/cm^2 to 78 μg/cm^2 (Figure 11, right), suggesting that the variation of specific area observed over this range was not due to significant changes in Pt.

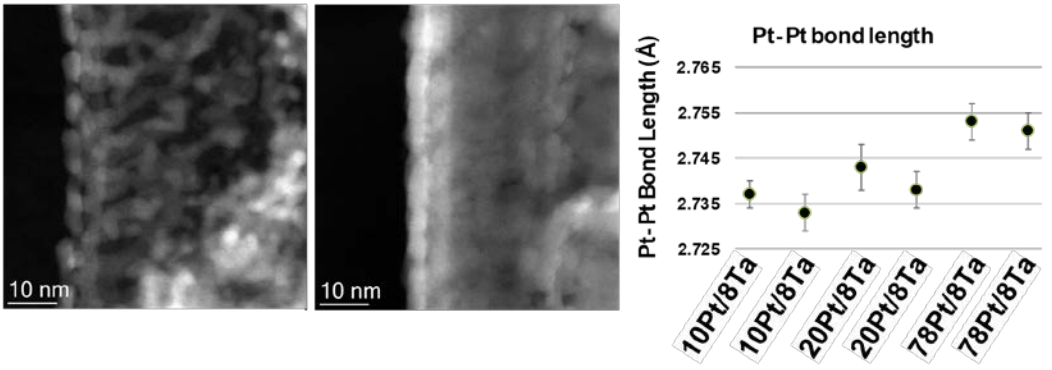

Figure 11. (Left and Center): STEM of 10Pt/8Ta/NSTF and 20Pt/8Ta/NSTF. (Right): XAFS-determined Pt-Pt bond lengths for 10Pt/8Ta, 20Pt/8Ta, and 78Pt/8Ta.

The primary hypothesis developed during the Pt/Ta/NSTF studies discussed above was that the loss of specific area and mass activity as the Pt loading on Ta decreased was due to low Pt utilization, imparted by insufficient electronic conductivity of the oxidized Ta layer and the discontinuous Pt surface coating. Experiments were conducted toward increasing the conductivity of the Ta underlayer, through modification of the Ta layer composition and changes to the catalyst processing. Figure 12 summarizes the impact of underlayer catalyst processing ("Previous" or "New") on catalyst activity and area. The "New" processing method resulted in significantly increased specific surface area relative to the "Previous" method, especially at low Pt areal loadings and concomitant thickness on Ta. With 10 $\mu g_{Pt}/cm^2$, the "New" processing method resulted in an approximate 4-fold gain in specific area, resulting in mass activity of 0.42 A/mg_{PGM}.

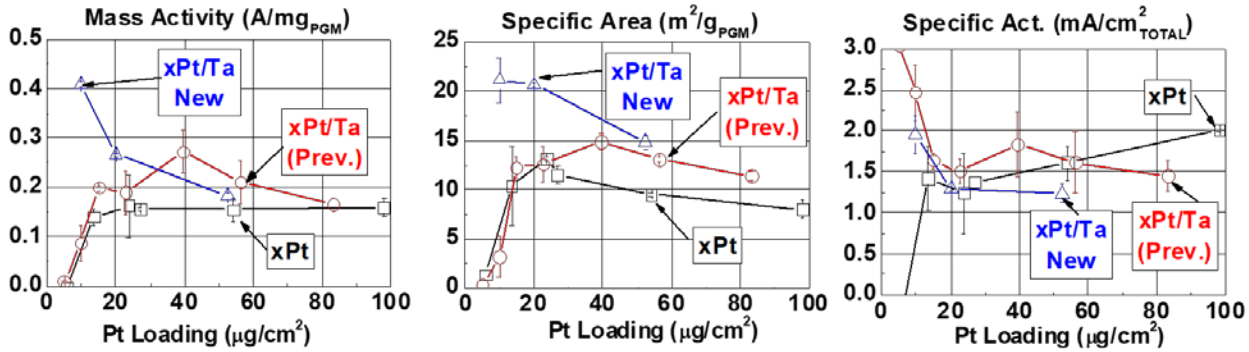

Figure 12. Mass activity, specific area, and specific activity of xPt/8Ta/NSTF with "Previous" and "New" processes

This year, work has been initiated toward development of an electrocatalyst durability model. DFT calculations were conducted to determine diffusion barriers for surface Pt atoms with different coordination levels and in the presence of oxide and hydroxide with a range of surface oxygen coverages. Additionally, interaction energies for Pt, Ni, and Ir over a range of compositions were calculated. The calculated diffusion barriers and interactions energies were integrated into a KMC model, which has been adapted to also include repeated oxidation and reduction cycles toward simulating the DOE electrocatalyst AST. Figure 13 compares a simulated defective Pt(111) surface to experiment in KOH electrolyte. Two-step oxidation is assumed, with formation of a "Pt-OH" species followed by formation of "Pt-O" species at higher potentials. The first peak (at ~0.75 V) is assumed to be associated with hydroxylation of Pt(111) terrace sites with coordination n = 9. Good agreement with experiment is seen when the second peak (at ~1.0 V) is found to be associated with step-edge and terrace vacancy edge oxidation to Pt-O. Upon reduction, reduced Pt-O species "pop out" of the terrace, simulating experimentally observed place exchange at higher potentials.

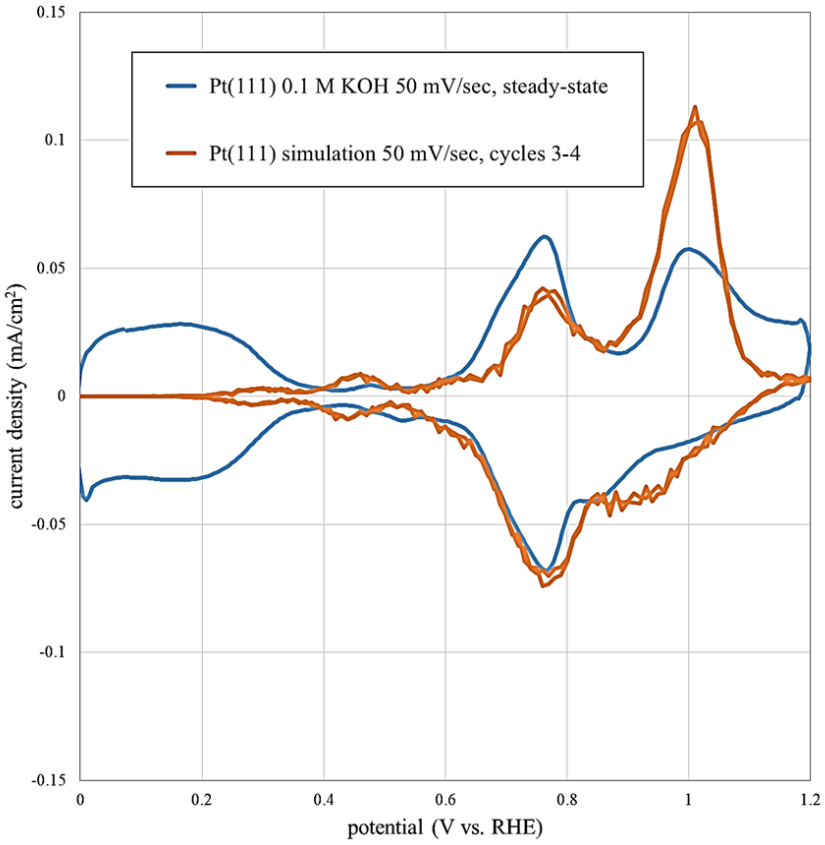

Figure 13. KMC simulation of Pt(111) oxidation and reduction as compared to experiment (0.1 M KOH)

Finally, development recently has been initiated toward implementation of NSTF catalysts and MEAs with improved break-in conditioning. STEM EDS and XAFS analysis of NSTF catalyst-coated membranes as a function of conditioning state reveal only subtle changes in composition and structure during this process. Studies also have identified that the break-in conditioning may be impacted by the slow removal of potential catalyst contaminants from the MEA during the conditioning process. Work is in progress to identify the sources of these potential contaminants and to confirm their impacts.

CONCLUSIONS AND UPCOMING ACTIVITIES

Over the past year, two UTF Pt/Ir/NSTF catalysts with ultra-low PGM content have been demonstrated that exceed five of the six DOE targets that this project addresses, and that achieve three of six of the more stringent project targets. Integration of an Ir layer between the surface Pt layer and the PR149 support has translated into significant gains in mass activity relative to pure Pt, due to increased specific area and, with some compositions, due to increased specific activity approaching values observed with highly active UTF PtNi alloys.

The Pt/Ir/NSTF catalysts are exceedingly durable toward electrocatalyst cycling, with several catalysts demonstrating mass activity losses of 20% or less and specific area losses of less than 10% after 30,000 potential cycles between 0.60 V and 1.0 V. The experimental activity and durability results are consistent with DFT simulations, which indicate high thermodynamic stability of Pt on Ir and the potential for increased specific activity, and KMC simulations, which indicate enhanced kinetic stability versus Ir-free systems. Integration of the durable Pt/Ir/NSTF catalysts with BOC components has resulted in demonstration of PGM contents of 0.106 g/kW to 0.110 g/kW at $Q/\Delta T$=1.45 kW/°C. Additionally, two surface-modified PtNi catalysts at optimal composition have produced PGM mass activities of 0.56 A/mg_{PGM} to 0.57 A/mg_{PGM}, via enhancement of specific activity as high as 3.0 mA/cm^2.

In future work, the project will continue the efforts toward development of one or more electrocatalysts that meet all DOE and project targets. This will be accomplished through further optimization of Pt and/or Pt-alloy surface catalysts on reduced-PGM content underlayers. Processing optimization of UTF catalysts on PGM-free underlayers also will continue, moving toward achieving entitlement of absolute and specific areas and mass activities with the underlayer approach. Simulation development will continue, with the objective of simulating a project Pt/Ir layered electrocatalyst through repeated potential cycling akin to the DOE AST and of additional screening of non-PGM underlayers. Lastly, work will continue to elucidate the factors responsible for break-in conditioning requirements with NSTF MEAs, and to identify and implement material solutions.

FY 2018 PUBLICATIONS/PRESENTATIONS

1. J. Greeley, "First principles studies of heterogeneous (electro)catalysis: incorporating structural complexity into catalyst reactivity and screening studies," Department of Physics, Central Michigan University, October 2017, Mount Pleasant, MI.
2. A.J. Steinbach, K.A. Lewinski, A.T. Haug, C. Duru, S.M. Luopa, G.M. Thoma, J. Park, F. Sun, A.E. Hester, J.T. Petrin, M.E. Kuznia, D.J. Myers, A.J. Kropf, D.A. Cullen, J. Greeley, Z. Zeng, and J. Erlebacher, "3M NSTF Electrocatalysts for PEM Fuel Cells and Water Electrolyzers," 232nd Meeting of The Electrochemical Society, Oct. 1, 2017, National Harbor, MD (Invited Plenary).
3. A.J. Steinbach, C. Duru, A.T. Haug, A.E. Hester, M.E. Kuznia, K.A. Lewinski, S.M. Luopa, J.T. Petrin, G.M. Thoma, A.J. Kropf, D.J. Myers, D. Yang, D.A. Cullen, J. Greeley, and Z. Zeng, "Ultrathin Film NSTF ORR Electrocatalysts for PEM Fuel Cells," *ECS Trans.* 80, no. 8 (2017): 659–676.
4. A.J. Steinbach, "Highly Active, Durable, and Ultra-low PGM NSTF Thin Film ORR Catalysts and Supports," USCAR Fuel Cell Tech Team, April 18, 2018, Detroit, MI.
5. A.J. Steinbach, Presentation FC143, 2018 Annual Merit Review, DOE Hydrogen and Fuel Cells Program, June 2018, Washington DC.
6. D.A. Cullen, D. Myers, J. Greeley, J. Erlebacher, G. Thoma, and A.J. Steinbach, "Exploring the Activity and Stability of Pt-based Catalysts through Analytical Electron Microscopy," Microscopy and Microanalysis, Baltimore, MD, August 5–9, 2018.
7. Z. Zeng, J. Kubal, A. Steinbach, and J. Greeley, "First principles electrocatalysis: perspectives on computational design of fuel cell electrocatalysts," Gordon Conference on Fuel Cells, August 2018, Smithfield, RI.
8. Z. Zeng, J. Kubal, A. Steinbach, and J. Greeley, "DFT studies of fuel cell electrochemistry," ECS Spring Meeting, October 2018, Cancun, Mexico.

REFERENCES

1. A.J. Steinbach, Presentation FC104, 2016 Annual Merit Review, DOE Hydrogen and Fuel Cell Vehicles Technology Programs, Washington DC, June 2016.
2. M.K. Debe et al., "Stop-Start and High-Current Durability Testing of Nanostructured Thin Film Catalysts for PEM Fuel Cells," *ECS Trans.* 3, no. 1 (2006): 835–853.
3. M.K. Debe et al., "Initial Performance and Durability of Ultra-Low Loaded NSTF Electrodes for PEM Electrolyzers," *J. Electrochem. Soc.* 159, no. 6 (2012): K165–K176.
4. M.K. Debe, "Tutorial on the Fundamental Characteristics and Practical Properties of Nanostructured Thin Film (NSTF) Catalysts," *J. Electrochem. Soc.* 160, no. 6 (2013): F522–F534.
5. A.J. Steinbach et al., "Highly Active, Durable, and Ultra-Low PGM NSTF Thin Film ORR Catalysts and Supports," 2017 Annual Project Progress Report to U.S. Department of Energy, Office of Energy Efficiency and Renewable Energy, Fuel Cell Technologies Office.